Supporting information

1. Sampling

The randomness of the sampling procedure safeguards the unbiasedness of the estimation, hence, great care must be giving to this step. The random selection of the sampled particles from the entire population are given by a slightly adapted version of a systematic uniform random sampling (SURS) procedure. In short, an automated SURS procedure is used: tilt series are recorded if:
- A particle is in the field of view
- A particle is partially in the field of view, but touching the upper part or right part of the field of view

In these two cases, the field of view was manually adjusted to bring the particle in the center of the field of view. Particles were not selected if:
- They were partially in the field of view, but touching the left part or bottom part of the field of view.
- If more than one particle was in the field of view, then the most near the center was chosen (least manual movement)
- Nearby gridbars cast shadows thereby limiting the tilt angle range resulting in poor tomographic reconstruction. Positions not allowing a 120° tilt range were excluded.

When the field of view was empty, no tilt series was recorded.
Practically, the SURS was carried out by a software (SerialEM) script:

```
// Distance 20 means that the stage shift between adjacent images will be 20 micrometer
Distance = 20
// Steps 5 means a grid of 4 x 4 (or 16 positions)
Steps = 4
// Information of where to save the data
SetDirectory D:\Data\Tomography Batch
SetNewFileType 1
OpenNewFile TomographyTilts.mrc

//Initialization, including homing of the holder to the goniometer 0,0 position (thereby steeing the first random
position)
Xsteps = $Steps
Ysteps = $Steps
Yback = 0
Counter = 0
Xstart = $Xsteps - 1
Xstart = $Xstart / 2
Xstart = -1 * $Xstart  * $Distance
Ystart = $Ysteps - 1
Ystart = $Ystart / 2
Ystart = -1 * $Ystart  * $Distance
MoveStageTo 0 0
MoveStage $Xstart $Ystart
Totalimage = $Steps * $Steps
Echo Starting

// Meandering through the 4 x 4 positional grid in a systematic and uniform procedure
Loop $Ysteps
    Loop $Xsteps
        G 1
        NormalizeLenses 7
        P
        S A
        Counter = $Counter + 1
        Echo $Counter of $Totalimage
        MoveStage $Distance 0
    EndLoop
    Xback = $Xsteps * $Distance * -1
```

```
    Yback = $Yback + $Distance
    MoveStage $Xback $Distance
EndLoop

CloseFile
MoveStageTo 0 0
Echo finished
```

The initial randomness is provided because:
- The deposition of particles during sample preparation process (drying) is random and beyond the control of the user;
- The grid rotation in the sample holder is random;
- The 0,0 position of the stage is not necessarily the center of the grid. The sample holder has a diameter depression of 3.5 mm into which the 3.05 mm grid loosely fits. This variation, 450 μm, is about 10 000 times the size of the objects under study.

Therefore, we can probably make the assumption that all particles have the same chance to be sampled.

2. Nanostars morphology
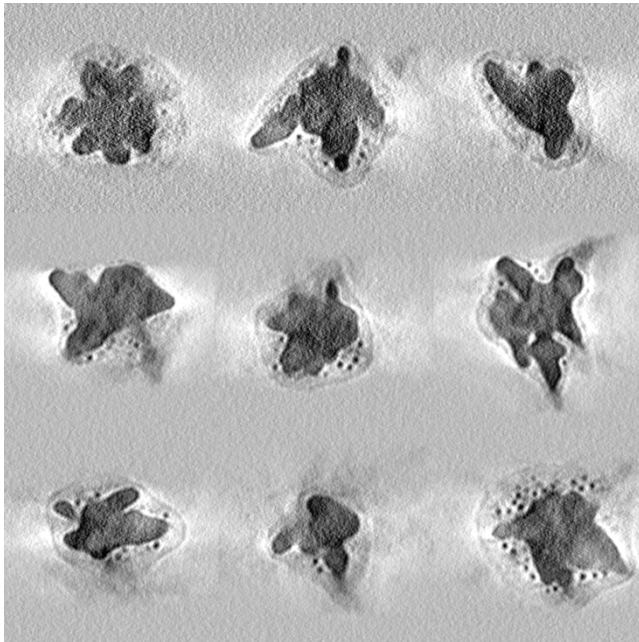
Figure SI-1. Orthogonal XY tomographic planes (thickness: 0.307 nm) through the first 9 Au nanostars. The dark signal of the particles is the effect of the strong electron scattering of Au. The enveloping polymer shell surrounding the particles is carbon-based and scatters much less strongly. The 5 nm round, dark particles inside the envelope are trapped fiducial markers (spherical Au nanoparticles) The bright artifacts, usually in the equatorial region of the particles are the effect of the under-sampling, originating in the technical impossibility to tilt over a 180° range.
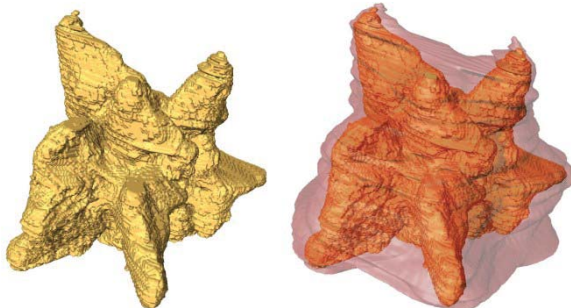

Figure SI-2. 3D rendering (by manually tracing) of an Au nanostar (left, yellow) and together with its surrounding PVP shell (right in red).

3. Holmes effect

The Holmes effect is an overprojection issue resulting in bias introduced if the slices are too thick: objects are seen as larger in projection since variations within the slice along the axial axis (the Z axis) are not considered, causing and their size to be overestimated. Estimators such as the Cavalieri volume estimator multiply the result of the probe count with the slice thickness and are therefore prone to the Holmes effect.

The projection of a perfect sphere will yield a circle in all orthogonal projections. However, the resolution along the axial dimension is a function of the slice thickness. Contained within one slice will project such object as a circle onto the XY plane, making it indiscernible from a cylinder. Hence, the volume will be overestimated by 27%. If the sphere is cut into 5 slices, the Holmes effect will be minimized since the upper and lower slices (the polar regions) will report lower areas. For a sphere cut into 5 equally-thick slices (1/5 or the dimeter), an overestimation of 16% can be contributed to the Holmes effect. Increasingly thinner slices will diminish the Holmes effect, until a theoretical infinitely thin slice thickness will eliminate the effect.
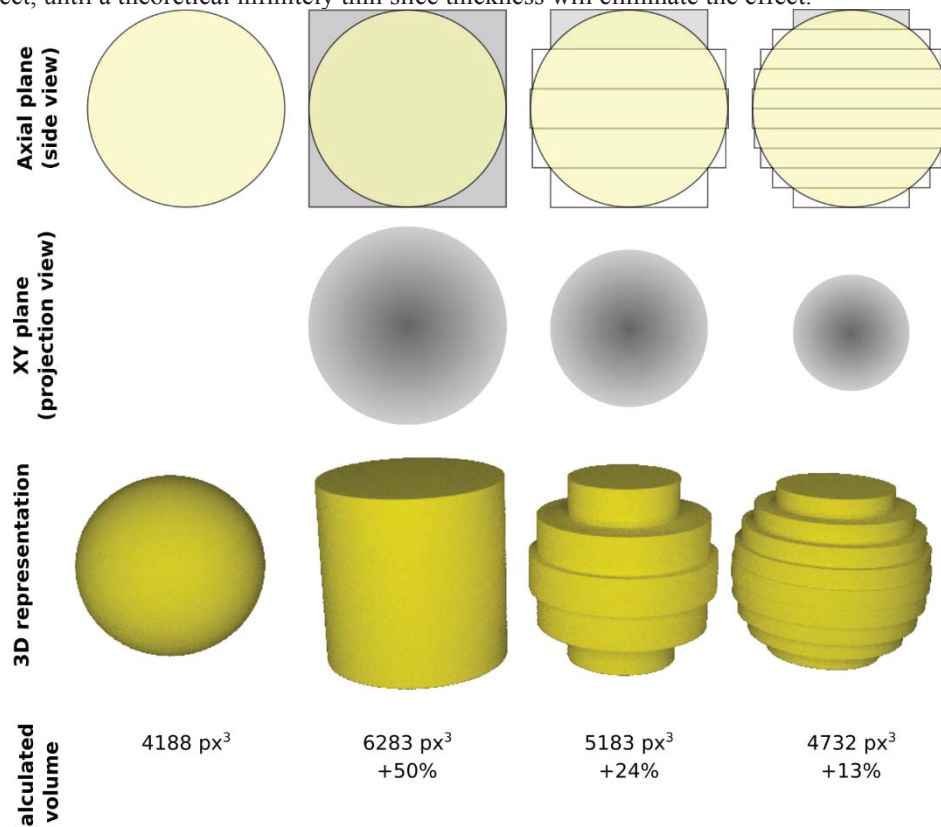
Figure SI-3. The Holmes effect. The estimate of the volume of a perfect sphere (radius = 10) is overestimated as a function of the axial resolution (the slice thickness). The schemes show the object in the axial plane (orthogonal side view, top), the projection of the top plane (second row), a 3D rendering of the modelled object (third row) and the estimated volume (bottom row). The mathematical computation is shown in the left column. A one-slice approach (second from left column) transforms the object essentially into a cylinder resulting in a large Holmes effect. Thinner slices (two rightmost columns)

model the sphere as a stack of thinner cylinders. The thinner the cylinder, the better it will resemble the mathematical sphere and the lower the volume overestimation.

Entirely overcoming the Holmes effect can be challenging but reducing it is not impossible. Subtracting the largest projected area was suggested (Gundersen, 1986) to remove most of the bias. Another possibility is to oversample along the z-axis, i.e. producing thinner planes and using not using every plane in the stereological analysis. It could be shown that using only every k^{th} section reduces the total Holmes effect by a factor k. The high resolution of the TEM provides a very small axial pixel size in the tomographic dataset (0.305 nm for the nanostars datasets). This is positive for two reasons: (1) it highly reduces the Holmes effect and (2) it allows a high k factors (practically, a k value of 15 was used for the nanostars, 12 for the aggregates), greatly increasing the efficiency of the analysis.

However, the concept of pixel size must not be confused with resolution. Axial resolution is a very tricky concept in tomography, which explain the general use of pixel size as surrogate. Conventionally, the resolution is calculated using the Crowther criterion(RA et al., 1970):

$$m = \frac{\pi \cdot D}{d}$$

Where m is the number of views, D is the size of the object (the diameter) and d is the resolution. For an approximately 40 nm particle, recorded with 61 views follows that d $\approx$ 2.06 nm. In fact, the distance u (see below) was chosen to be larger than the axial resolution in order to avoid issues with resolving structures between planes.

4. Example the procedure with one nanostars, including calculation of the coefficient of error for the Cavalieri probe.

The 3D tomographic dataset is a set of parallel section planes with a constant separation t. The set of section planes is randomly positioned on the object, i.e. the first section to hit the object is random within an interval of length t. Note that since the set of sections must have a random position on the object, the number of planes of thickness t containing something of the object is a random variable and not the same for each orthogonal dimension.

By convention, the orientation of the planes in the 3D tomographic dataset when opened are known as the XY plane. The following script was then applied to each dataset. The output is single stack containing the object sliced in XY, XZ and YZ plane, reduced along the z-axis with a resolution (4.6 nm) matching the distances between crosses (4.6 nm, area per cross = 4.6^2 nm = 20.2 nm^2) and the distance between lines (4.6 nm). The one-stack option allows to analyze the three orthogonal dimensions most efficiently, ie. Without open and closing data and therefore without the need to take the attention away from the data. The green crosses and magenta lines overlay allow to perform both a fakir probe and Cavalieri point count with the same dataset. The script was written in ImageJ and is understood as IJ1 macro. It assumes the tomogram is open.

```
// open data
rename("XYplane");

// Duplicate into 3 orthogonal planes: XY, XZ and YZ;
//================================================
// XY to XZ plane
run("Duplicate...", "title=XZplane duplicate");
selectWindow("XZplane");
run("Reslice [/]...", "output=0.307 start=Left avoid");
selectWindow("XZplane");
close();
selectWindow("Reslice of XZplane");
rename("XZplane");

// XY to YZ plane
selectWindow("XYplane");
run("Duplicate...", "title=YZplane duplicate");
selectWindow("YZplane");
run("Reslice [/]...", "output=0.307 start=Top avoid");
selectWindow("YZplane");
close();
selectWindow("Reslice of YZplane");
rename("YZplane");
```

```
    // Concatenate the three stacks into one z-stack
    run("Concatenate...", "   title=[Concatenated  Stacks]  image1=XYplane  image2=XZplane
image3=YZplane image4=[-- None --]");

    //Reduce the Z resolution (k factor = 15) and assure the XY resolution is correct
    selectWindow("Concatenated Stacks");
    run("Reduce...", "reduction=15");
    run("Set Scale...", "distance=3.2573 known=1 pixel=1 unit=nm");

    // Place colored overlays
    run("Grid...", "grid=Crosses area=21.2 color=Green");
    run("Flatten", "stack");
    run("Grid...", "grid=[Horizontal Lines] area=21.20 color=Magenta");
    run("Flatten", "stack");
```

The resulting stack can be immediately interpreted according to the following convention. Incidents of the magenta lines (the fakir probe) crossing the object are counted as line intercepts and events of a cross (produced by the short green vertical line and the magenta line) on the object are count as (Cavalieri) points. In the zoom-in depicted below, most events are straightforward to interpret, with the exception of incidents involving the round small object on the left and the line crossing second from bottom on the right (open cyan arrowhead). The small round object of the first case is a fiducial marker and is not part of the object. Hence, the interpretation is to disregard these events (two line interceps, one cross point). The corss of the second case may be interpreted as edge-on. In such a case, the operator must faithfully interpret the situation. Here, it was decided that the cross was inside the object and therefore it was counted. In situations where one pixel may decide, and thus exceeding the precision of the cross, which is hiding the pixel underneath, the pixel in the upper left corner of the cross was used. the results of this selection are 10 line intercepts (yellow open arrows) and 13 point counts (cyan arrowheads).
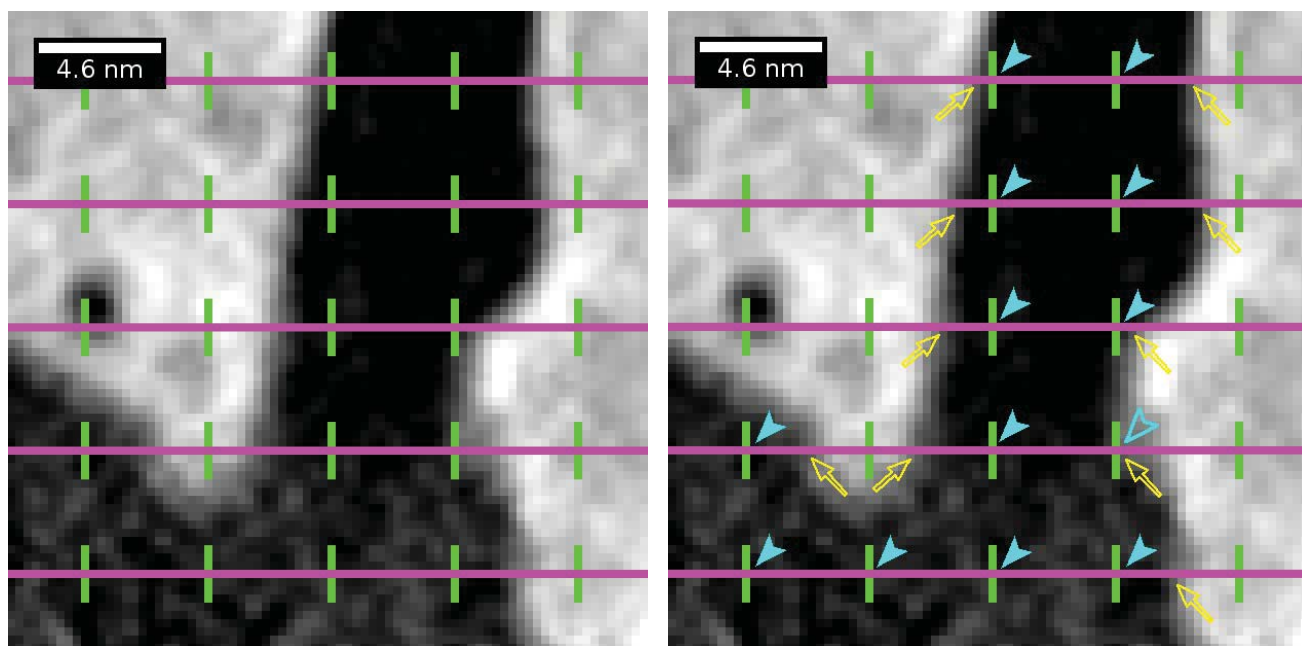
Figure SI-4. Line counting and point counting on a zoomed-in part of a plane.

The sweeping tangent method comprises the visual inspection of the plane and detecting the number of occations of convex and concave curves with respect to the horizon. In the example below, the red lines denote where the object is curves outward (i.e. convex) and the green lines denote hollowed out, convex incidents (with the horizon as reference).
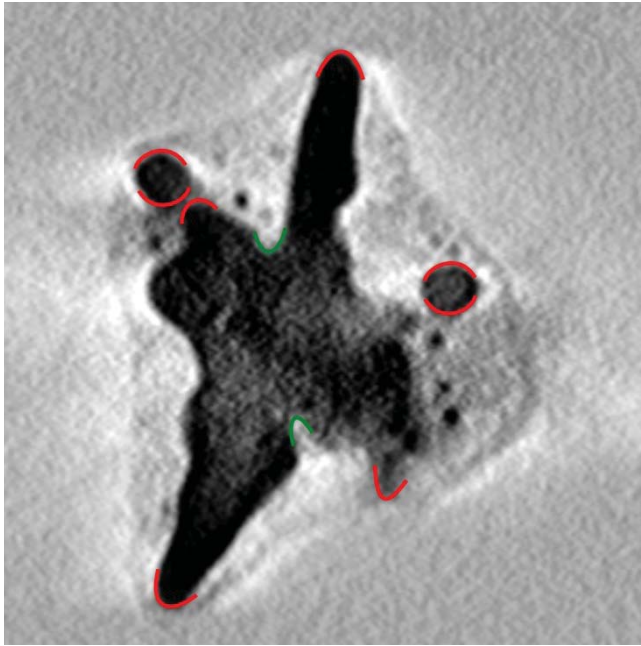
Figure SI-5. Tangent sweep probe of a plane.

These three probes are applied to each 15th slide (the k factor) of the object:
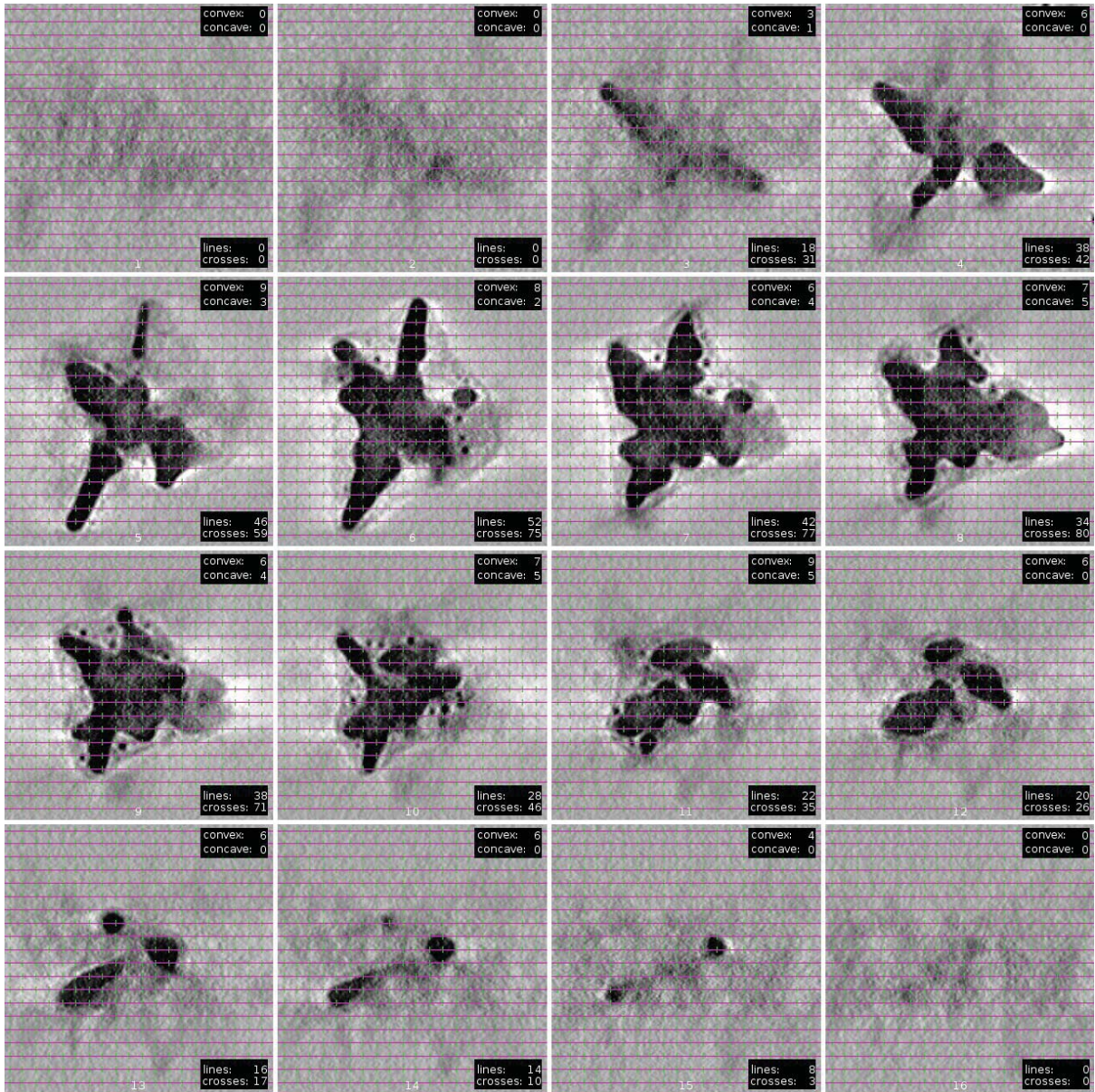
Figure SI-6. Line counting, point counting and tangent sweep counting on an entire object. In the XY plane, a total of 376 line interceps and 492 cross pints were registered. The sweeping tangent yielded 83 convex and 29 concave events.

The procedures are repeated for the XZ plane:
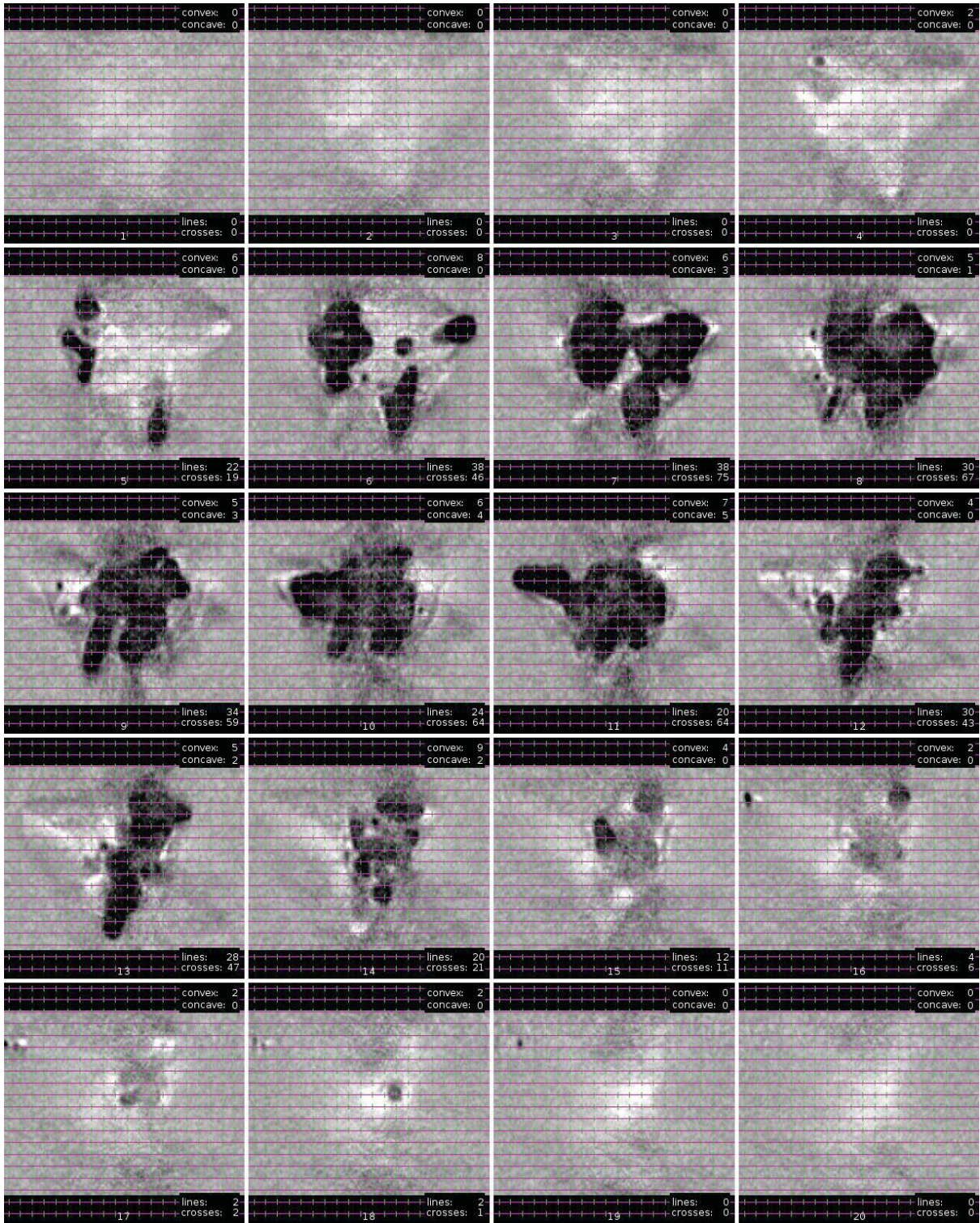
Figure SI-7. Line counting, point counting and tangent sweep counting on an entire object. The XZ plane yielded a total line intercept count of 302, whereas the crosses count was 524. The sweeping tangent count yielded 73 convex and 20 concave events.

A final repetition in the YZ plane is performed. The YZ planes are the ones suffering the most from the missing wedge effect, which renders them most prone to interpreter bias.

**Figure SI-8. Line counting, point counting and tangent sweep counting on an entire object. On the YZ plane a total line intercept count of 320, whereas the crosses count was 505. 76 convex and 19 concave incidents were counted.**

The above three panels (SI-6, SI-7 and SI-8) are availble at a high resolution for closer inspection. All the counts are summarized in the table below.

	Line intercepts			Cross points			Sweeping tangent (convex / concave)		
Plane	**XY**	**XZ**	**YZ**	**XY**	**XZ**	**YZ**	**XY**	**XZ**	**YZ**

1	18	22	2	31	19	2	3 / 1	2 / 0	2 / 0
2	38	38	6	42	46	3	6 / 0	6 / 0	2 / 0
3	46	38	8	59	75	6	9 / 3	8 / 0	2 / 0
4	52	30	14	75	67	9	8 / 2	6 / 3	4 / 0
5	42	34	20	77	59	16	6 / 4	5 / 1	14 0
6	34	24	32	80	64	45	7 / 5	5 / 3	10 / 3
7	38	20	28	71	64	50	6 / 4	6 / 4	4 / 2
8	28	30	38	46	43	62	7 / 5	7 / 5	6 / 2
9	22	28	32	35	47	70	9 / 5	4 / 0	6 / 4
10	20	20	36	26	21	69	6 / 0	5 / 2	7 / 3
11	16	12	30	17	11	70	6 / 0	9 / 2	6 / 4
12	14	4	42	10	6	75	6 / 0	4 / 0	7 / 1
13	8	2	32	3	2	28	4 / 0	2 / 0	6 / 0
14		2	18		1	17		2 / 0	4 / 0
15			14			12			2 / 0
16			6			5			2 / 0
17			4			2			2 / 0
Total	**376**	**302**	**320**	**572**	**524**	**505**	**83 / 29**	**69 / 20**	**76 / 19**

Table SI-1. Summary of the counts (Line intersect, Cavalieri counts, Tangent sweep) on one entire object.

Surface estimation

The unbiased surface area estimation is based on the random intersection of the geometrical fakir probe (the horizontal magenta lines), which is an isotropic set of parallel lines with a spacing of $u=4.6$ nm through the 3D object. The parallel lines transect the object. The surface area is then given by

$$Est(S) = \frac{2}{d} \cdot u^2 \cdot \sum_{1}^{n} (I_{xy} + I_{xz} + I_{yz})$$

Where d the number of dimensions (=3), u the length between two parallel test lines (=4.6 nm) and I_{xy}, I_{xz} and I_{yz} the total number of intersections between the object and the fakir probe over the n planes. The surface of the example can therefore be estimated by:

$$Est(S) = \frac{2}{3} \cdot 4.6^2 \cdot \sum_{1}^{17} (376 + 302 + 320) = 14\ 109\ nm^2$$

Volume estimation

For unbiased volume estimation the Cavalieri probe is required: points (generated by the intersection of the magenta fakir probe lines with vertical short green lines at the same spacing u fall on the object of interest and are counted. This total sum of these counts relates to the volume of the object according to:

$$Est(V) = \frac{1}{d} \cdot \sum_{1}^{n} P_i \cdot A_p \cdot u$$

Where P_i the total number of points falling on the particle in plane i, n is the total number of planes (17), u is the thickness of the planes (4.6 nm), and A_p is the associated area per point ($u^2 = 21.2\ nm^2$). This yields for the example above:

$$Est(V) = \frac{1}{3} \cdot \sum_{1}^{17} (572 + 524 + 505) \cdot 20.2 \cdot 4.6 = 49\ 587\ nm^3$$

The precision of the estimate, expressed by the coefficient of error (CE), is quite challenging: variance estimators such as coefficient of error are only valid for n *independent* observations. However, a strong dependence between areas of systematic sections exists, even from very irregularly shaped objects: if a

particular section in the systematic series happens to be relatively large then very likely the previous and the following sections will also be large.

We used the solution proposed by Gundersen and Jensen. (Gundersen and Jensen, 1987) In short: 3 factors A, B and C are calculated for each plane, taking into account the changes in subsequent planes. A is the number of points counted squared ($(P_i)^2$). B is the number of points multiplied with the number of points on the next plane ($P_i \cdot P_{i+1}$) and C is the number of points multiplied with the number of points of the plane after that (($P_i \cdot P_{i+2}$).

Plane	Counts XY	A	B	C	XZ	A	B	C	YZ	A	B	C
1	31	961	1302	1829	19	361	874	1425	2	4	6	12
2	42	1764	2478	3150	46	2116	3450	3082	3	9	18	27
3	59	3481	4425	4543	75	5625	5025	4425	6	36	54	96
4	75	5625	5775	6000	67	4489	3953	4288	9	81	144	405
5	77	5929	6160	5467	59	3481	3776	3776	16	256	720	800
6	80	6400	5680	3680	64	4096	4096	2752	45	2025	2250	2790
7	71	5041	3266	2485	64	4096	2752	3008	50	2500	3100	3500
8	46	2116	1610	1196	43	1849	2021	903	62	3844	4340	4278
9	35	1225	910	595	47	2209	987	517	70	4900	4830	4900
10	26	676	442	260	21	441	231	126	69	4761	4830	5175
11	17	289	170	51	11	121	66	22	70	4900	5250	1960
12	10	100	30	0	6	36	12	6	75	5625	2100	1275
13	3	9	0	0	2	4	2	0	28	784	476	336
14					1	1	0	0	17	289	204	85
15									12	144	60	24
16									5	25	10	0
17									2	4	0	0
Total	572	33616	32248	29256	524	28925	27245	24330	505	30187	28392	25663

Table SI-2. Calculation of the factors required in the calculation of the coefficient of error.

These three factors can be inserted in the formula for the components of the coefficient of error (adapted from (Gundersen and Jensen, 1987)). The two components are noise and variation due to sampling (VAR_{SURS}):

$$Noise = 0.0724 \cdot \frac{b}{\sqrt{a}} \cdot \sqrt{n \cdot \sum_{1}^{n} P_i}$$

$$VAR_{SURS} = \frac{(3 \cdot (A - noise) - 4 \cdot B + C)}{240}$$

Where n is the number of planes and the factor $\frac{b}{\sqrt{a}}$ is the boundary length of the object in a plane divided by the root of the area of the object in that plane. The boundary length for each plane was extracted using the ImageJ "Analyze particles" routine (where it is called "Perimeter"). This routine also delivers the area of the objects in each plane. The area was already found using the stereological approach: $P_i \cdot A_p$ results in the estimated area. The total variation is the sum of these two components and the coefficient of error (CE), is the calculated as:

$$CE = \frac{\sqrt{noise + VAR_{SURS}}}{\sum_{1}^{n} P_i}$$

From the above example, the noise, VAR_{SURS}, total variation and CE was calculated for each orthogonal dimension:

	noise	VAR_{SURS}	Total	CE

			Variation	
XY	34.9	4.20	39.1	1.09%
XZ	34.7	8.42	43.1	1.25%
YZ	38.8	10.6	49.4	1.30%
Average	**36.2**	**7.73**	**43.9**	**1.21%**

Table SI-3. The **coefficient of error for one object, dissected into its components for each orthogonal dimension.**

The coefficient of error (CE) was calculated for the example volume estimate at 1.21%, based on a total of 1638 point counts (572 in XY, 525 in XZ and 541 in YZ). The missing wedge effect causes a higher variation in XZ and especially in YZ, where the effect is the strongest. In average over the three dimensions, 82.4% of the variation derives from the noise (and 17.6% from the sampling).

Curvature estimation

Curvature, and in particular the integrated mean curvature in its normalized form (M is defined as the algebraic average of the two curvatures in each point on the surface integrated over the surface), is obtained by a tangent count(Dehoff): a horizontal line is swept down across each orthogonal slide and sites of tangents with convex (T_{cx}, dotted yellow in figure 2D) and concave (T_{cc}, dashed green line in Figure 2D) boundaries are counted. M_v is the volume corrected integral mean curvature. The M_v is calculated as:

$$Est(M_v) = \frac{1}{d} \cdot \frac{\pi}{Est(S)} \cdot \sum_{1}^{n} T_{cx} - T_{cc}$$

$$Est(M_v) = \frac{1}{3} \cdot \frac{\pi}{14109} \cdot \sum_{1}^{n} 228 - 68 = 11\,875\,\frac{\mu m}{\mu m^3}$$
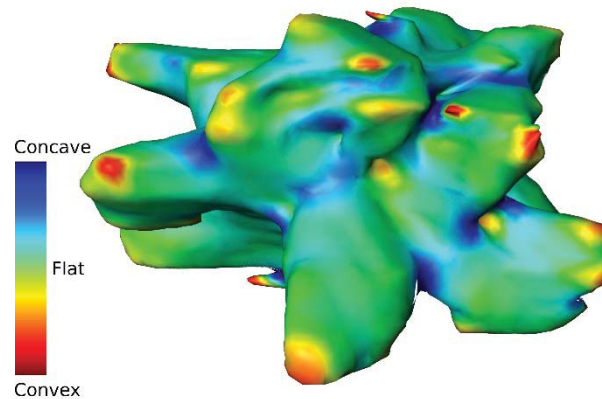

Figure SI-9. Falso-colored 3D rendering of an Au nanostars. The color represents local curvature (Blue: concave, Red, Conves)

5. Thermal reshaping of Au nanostars
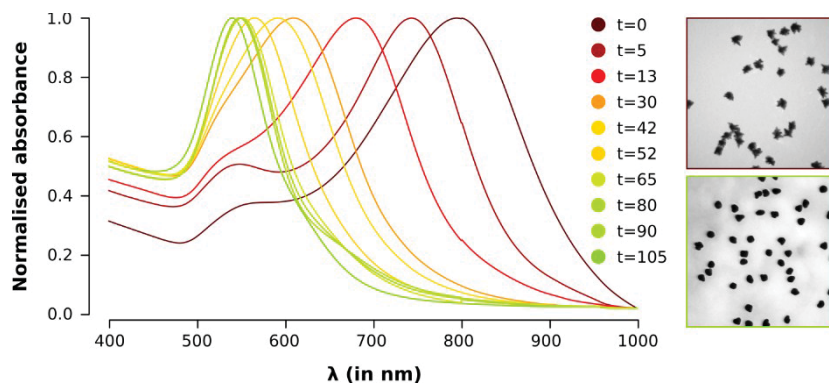
Figure SI-10. Spectral evolution of Au nanostars subjected at thermo-treatment: 140 °C in DMF. Right: TEM images of Au nanostars before (top) and after (bottom) thermal reshaping.

6. Simulation scripts

The object was simulated in ImageJ macro language according to the following code:

```
newImage("Untitled", "8-bit black", 400, 400, 400);

//fiducials
fiducial=50;


// shell
stack_depth=400;
Max_radius=300;  //diameter
start_color=140;
end_color=40;
step=(start_color-end_color)/Max_radius;
gray_range=start_color;
starting_slice=(stack_depth/2-Max_radius/2);
for (e=starting_slice;e<Max_radius+starting_slice+1;e++){
    setSlice(e);
    radius=sqrt(abs(Max_radius*Max_radius)-( (Max_radius-2*( e-
starting_slice))* (Max_radius-2*( e-starting_slice))));
    gray_range=abs(gray_range-step);
    setForegroundColor(gray_range,gray_range,gray_range);
    makeOval(stack_depth/2-(radius/2), stack_depth/2-(radius/2),radius,
radius);

    if (radius > 0) {
        run("Fill", "slice");
    }
}

// particle
stack_depth=400;
Max_radius=200;  //diameter
start_color=255;
end_color=60;
step=(start_color-end_color)/Max_radius;
gray_range=start_color;
starting_slice=(stack_depth/2-Max_radius/2);
for (e=starting_slice;e<Max_radius+starting_slice+1;e++){
    setSlice(e);
```

```
        radius=sqrt(abs(Max_radius*Max_radius)-( (Max_radius-2*( e-
starting_slice))* (Max_radius-2*( e-starting_slice))));
        gray_range=abs(gray_range-step);
        setForegroundColor(gray_range,gray_range,gray_range);
        makeOval(stack_depth/2-(radius/2), stack_depth/2-(radius/2),radius,
radius);
        if (radius > 0) {
                run("Fill", "slice");
        }
}

// fiducials
stack_depth=400;
Max_radius=50;
setForegroundColor(255, 255, 255);
X_shift=100;
Y_shift=100;
for (e=1;e<stack_depth+1;e++){
        slice=(stack_depth-Max_radius/2)-((stack_depth-Max_radius))+e/2;
        setSlice(slice);
        radius=sqrt(abs(Max_radius*Max_radius)-((Max_radius-e)*(Max_radius-
e)));
        makeOval(X_shift+(stack_depth-radius)/2,Y_shift+(stack_depth-
radius)/2,radius, radius);
        if (radius > 0) {
                run("Fill", "slice");
        }
}

stack_depth=400;
Max_radius=50;
setForegroundColor(255, 255, 255);
X_shift=100;
Y_shift=-100;
for (e=1;e<stack_depth+1;e++){
        slice=(stack_depth-Max_radius/2)-((stack_depth-Max_radius))+e/2;
        setSlice(slice);
        radius=sqrt(abs(Max_radius*Max_radius)-((Max_radius-e)*(Max_radius-
e)));
        makeOval(X_shift+(stack_depth-radius)/2,Y_shift+(stack_depth-
radius)/2,radius, radius);
        if (radius > 0) {
                run("Fill", "slice");
        }
}

stack_depth=400;
Max_radius=50;
setForegroundColor(255, 255, 255);
X_shift=-100;
Y_shift=-100;

for (e=1;e<stack_depth+1;e++){
        slice=(stack_depth-Max_radius/2)-((stack_depth-Max_radius))+e/2;
        setSlice(slice);
        radius=sqrt(abs(Max_radius*Max_radius)-((Max_radius-e)*(Max_radius-
e)));
        makeOval(X_shift+(stack_depth-radius)/2,Y_shift+(stack_depth-
radius)/2,radius, radius);
        if (radius > 0) {
                run("Fill", "slice");
```

```
        }
}
stack_depth=400;
Max_radius=50;
setForegroundColor(255, 255, 255);
X_shift=fiducial;
Y_shift=fiducial;
Z_shift=300;
for (e=1;e<stack_depth-Z_shift;e++){
      slice=(-1/2)*Max_radius+Z_shift+(stack_depth-Max_radius/2)-
((stack_depth-Max_radius))+e/2;
      setSlice(slice);
      radius=sqrt(abs(Max_radius*Max_radius)-((Max_radius-e)*(Max_radius-
e)));
      makeOval(X_shift+(stack_depth-radius)/2,Y_shift+(stack_depth-
radius)/2,radius, radius);
      if (radius > 0) {
            run("Fill", "slice");
      }
}

stack_depth=400;
Max_radius=50;
setForegroundColor(255, 255, 255);
X_shift=-1*fiducial;
Y_shift=fiducial;
Z_shift=300;
for (e=1;e<stack_depth-Z_shift;e++){
      slice=(-1/2)*Max_radius+Z_shift+(stack_depth-Max_radius/2)-
((stack_depth-Max_radius))+e/2;
      setSlice(slice);
      radius=sqrt(abs(Max_radius*Max_radius)-((Max_radius-e)*(Max_radius-
e)));
      makeOval(X_shift+(stack_depth-radius)/2,Y_shift+(stack_depth-
radius)/2,radius, radius);
      if (radius > 0) {
            run("Fill", "slice");
      }
}

stack_depth=400;
Max_radius=50;
setForegroundColor(255, 255, 255);
X_shift=fiducial;
Y_shift=-1*fiducial;
Z_shift=300;
for (e=1;e<stack_depth-Z_shift;e++){
      slice=(-1/2)*Max_radius+Z_shift+(stack_depth-Max_radius/2)-
((stack_depth-Max_radius))+e/2;
      setSlice(slice);
      radius=sqrt(abs(Max_radius*Max_radius)-((Max_radius-e)*(Max_radius-
e)));
      makeOval(X_shift+(stack_depth-radius)/2,Y_shift+(stack_depth-
radius)/2,radius, radius);
      if (radius > 0) {
            run("Fill", "slice");
      }
}

stack_depth=400;
Max_radius=50;
```

```
setForegroundColor(255, 255, 255);
X_shift=-1*fiducial;
Y_shift=-1*fiducial;
Z_shift=300;
for (e=1;e<stack_depth-Z_shift;e++){
      slice=(-1/2)*Max_radius+Z_shift+(stack_depth-Max_radius/2)-
((stack_depth-Max_radius))+e/2;
      setSlice(slice);
      radius=sqrt(abs(Max_radius*Max_radius)-((Max_radius-e)*(Max_radius-
e)));
      makeOval(X_shift+(stack_depth-radius)/2,Y_shift+(stack_depth-
radius)/2,radius, radius);
      if (radius > 0) {
          run("Fill", "slice");
      }
}
```

7. Detailed result for all Au nanostars

Nanostars			
Particle #	Surface	Volume (CE)	Curvature
1	9288.2	34 732.2 (1.73%)	0.027 8
2	11182.6	40 168.2 (1.38%)	0.020 1
3	8015.9	27 798.8 (1.69%)	0.025 8
4	8468.3	32 876.8 (1.66%)	0.022 8
5	7040.4	29 914.6 (2.18%)	0.018 9
6	7648.3	19 726.1 (1.5%)	0.031 1
7	10 532.3	33 820.7 (1.50%)	0.023 9
8	13 741.5	45 181.1 (1.30%)	0.023 1
9	10 334.4	35 708.7 (1.67%)	0.020 0
10	11 126.1	32 811.7 (1.37%)	0.024 5
11	12 016.7	39 680.0 (1.85%)	0.023 5
12	8284.5	30 272.7 (1.25 %)	0.027 0
13	8397.6	50 226.6 (1.75%)	0.031 5
14	9274.1	33 853.3 (1.77%)	0.020 1
15	9500.3	35 480.9 (1.77%)	0.025 6
16	10 292.0	39 126.6 (1.49%)	0.025 3
Mean	9696.5 nm^2	35 086.2 nm^3 (1.62 %)	0.024 4 nm/nm^3
SD	1772.1 nm^2	7219.9 nm^3	0.003 9 nm/nm^3

Figure SI-4. Volume, surface and mean local curvature for all nanostars in the study.

8. Detailed result for all Au nanospheres

Nanospheres			
Particle #	Surface	Volume (CE)	Curvature
1	6833	45 511 (2.72%)	0.014 1
2	6990	37 675 (3.05%)	0.014 1
3	5341	29 688 (4.28%)	0.017 1
4	7226	47 320 (2.73%)	0.016 0
5	7618	59 225 (2.23%)	0.014 5

6	8011	52 594 (2.45%)	0.016 8
7	7933	52 896 (2.44%)	0.015 7
8	8561	56 965 (2.32%)	0.014 7
9	7147	44 004 (2.80%)	0.017 8
10	7383	42 950 (2.79%)	0.016 2
11	7697	50 485 (2.49%)	0.013 3
12	7304	47 018 (2.77%)	0.015 7
13	7304	48 073 (2.49%)	0.015 7
14	6362	35 415 (3.20%)	0.015 4
15	7226	45 662 (2.71%)	0.014 1
16	5733	30 743 (3.53%)	0.020 5
17	6833	36 469 (3.16%)	0.016 6
18	6755	38 881 (2.95%)	0.017 8
19	6833	42 648 (2.74%)	0.016 2
20	8482	54 252 (2.46%)	0.017 8
Mean	**7179 nm^2**	**44 923 nm^3 (2.82%)**	**0.016 0 nm/nm^3**
SD	**799 nm^2**	**8287 nm^3**	**0.001 7 nm/nm^3**

Figure SI-5. Volume, surface and mean local curvature for all spherical nanoparticles in the study.

## 9. Precision of the stereological estimates of nanostars surface
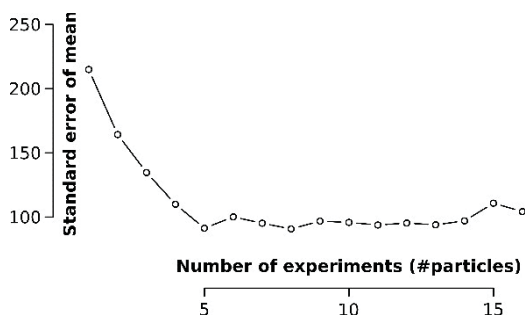
Figure SI-11. Development of the standard error of mean of the surface area (estimated by the Fakir probe) with increasing number of experiments (particles). After 5 Au nanostars, no further reduction of SEM is observed.

10.   Size analysis of single Au nanospheres used in aggregates

25 images were recorded automatically recorded in SURS fashion (SI-11A), imported in ImageJ and thresholded (SI-11B) using the default setting. The analysis modelled the particles as ovals and calculated the major and minor axes (SI-11C). Finally, a histogram plot of half the major axis, as a marker for the particle radius, of 27363 particles (line in SI-11D) was plotted above the histogram of the radii estimated by the Cavaieri probe (n=48). The number of bin adapted to the number of observations (n) using the following this function $B = \sqrt{n}$. There is no significant difference.
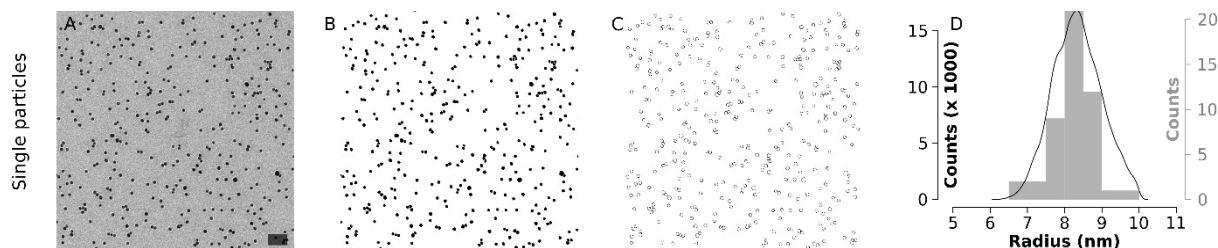
Figure SI-12. TEM micrograph (A), thresholded (B) and modelled (C) of one of 25 images used for the radius calculation from single particles. The histograms for major axis of single, non-aggregated particles (line) overlaps with the box histogram of particle radius inside the aggregate.

11. Sandbox method for fractal dimension in 3D
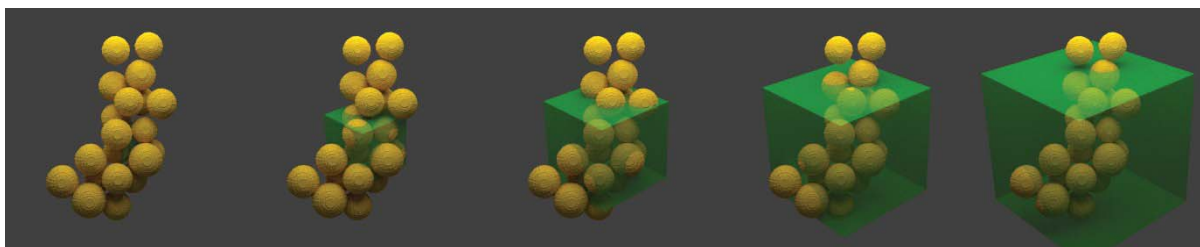
Figure SI-13. Graphical representation of the expansion of the sandbox method in 3D. The volume of the aggregate is assessed within each box. The fractal dimension is a function of the natural logarithm of the aggregate's volume within each box, plotted against the natural logarithm of the volume of that box.

12. Time and resources

All tomographic recordings and stereological analysis were performed by one person. The time and resources required for these experiments according to these categories:

Sample preparation

It is assumed that the objects are available at the start of the quantification steps. The preparation of the objects (by dropcasting or nebulization) takes little time, but a sufficient long period of time must be allowed for drying (3h), as no water may enter the transmission electron microscope. No special instruments are required.

Data recording / 3D reconstruction

The recording of a single tilt series takes about 30 minutes and is automated. The alignment and reconstruction requires hands-on action and takes about the same period of time. Ideally, the first tilt series is reconstructed by the time the second tilt series has finished its recording. Working this efficiently, about 16 datasets can be recorded in a typical day. A conventional TEM and an up-to-date PC are required.

Once the datasets are recorded, a decision must be made on variables in the stereological analysis. In particular, the area per point, the distance between lines and the k factor influence the time needed to analyze the data and the final precision. This step also includes the design of the spreadsheet data. Estimated time: a half day per study. A normal laptop sufficed.

Stereological analysis

Once setup, the analysis per se is a comparatively short affair. The use of a mechanical click-counter tool makes the procedure even more efficient. The counts were entered in spreadsheet software, which was the most demanding step, as it may take concentration the analysis itself. In average, about 10 minutes per Au nanostars were needed, or less than 3 hours for the entire study. The analysis of the Au aggregates was performed within 1 day, since the precision was chosen to be lower and smaller aggregates were processed faster. A normal laptop sufficed.

Summarizing data

Finally, the data is summarized spreadsheet and formulas, e.g. for the calculation of the CE, as programmed in the spreadsheet. Time required: 1 hour. A normal laptop sufficed.

1: 1 day

2: 2 days

3 1 day

4 2 days

5 2 days

13. Agreement of fractal dimension measurement

The Bland-Altman plot is used to show the agreement between the two methods used (Cavalieri estimate and scaling) to estimate the fractal dimension. The mean difference between the methods is 0.08.
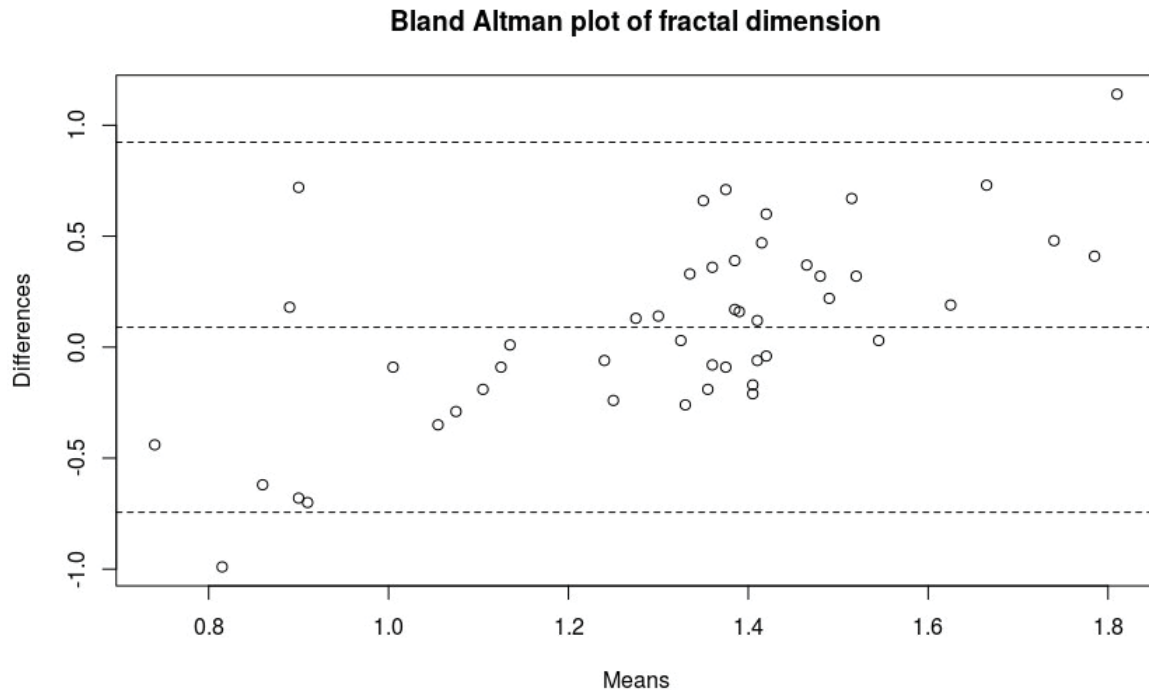
Figure SI-14. Bland-Altman plot of the results of the two methods used to estimate the fractal dimension. The upper and lower dotted lines denote 1.96 standard deviations. The central line the mean difference between the methods.

The Students't test was used to assess significant differences between the two sets of results. The prerequisites for the Student's t test were fulfilled: normal distribution (Saphiro-Wilk test: W=0.97361, p=0.3609 for the Cavalieri estimates) and independent from each other. The statistic t was calculated at 1.3101, with a p value of 0.1948.

References

Dehoff, R.T. Stereological uses of the tangent count. In Geometrical Probability and Biological Structures: Buffon's 200th Anniversary., (Springer Verlag, Berlin), p.

Gundersen, H.J.G. (1986). Stereology of arbitrary particles*: A review of unbiased number and size estimators and the presentation of some new ones, in memory of William R. Thompson. Journal of Microscopy *143*, 3–45.

Gundersen, H.J.G., and Jensen, E.B. (1987). The efficiency of systematic-sampling in stereology and its prediction. Journal of Microscopy-Oxford *147*, 229–263.

RA, C., DJ, D., and A, K. (1970). Reconstruction of 3-dimensional structure from projections and its application to electron microscopy. Proceedings of the Royal Society of London Series A: Mathematical and Physical Sciences *317*, 319–340.